Laser vibrometer condition assessment of cemented materials using wavelet synchro-squeezed transform

Piotr Wiciak[1,*], Giovanni Cascante[1], and *Maria Anna Polak*[1]
[1]Univeristy of Waterloo, Department of Civil and Environmental Engineering, Waterloo, Ontario, Canada

Abstract. Current non-destructive ultrasonic techniques (NDT) are based mostly on wave velocity analysis. While current techniques can identify severe damage, they fail to detect early deterioration. Therefore, the proposed method, based on the propagation of surface waves, takes into account not only changes in wave velocity but also changes in wave attenuation. In practical/field applications, access to a structure is often limited to one side only (i.e. concrete slabs, vacuum building walls). Thus, surface wave analysis is a natural solution. To improve the reliability of wave attenuation measurements, responses of ultrasonic transducers are measured using a high-frequency Doppler laser vibrometer. Firstly, the ultrasonic transducer is characterized using the laser vibrometer. Then, based on the sensitive frequency ranges, response signals measured for the cemented sand specimen are analyzed, and the relative attenuation index based on spectral energy is proposed. The method is further improved using the wavelet synchro-squeezed transform.

1 Introduction

The condition of structural materials in civil engineering applications is critical for the safety of structures. The most popular ultrasonic non-destructive techniques, used for the evaluation of the structural material condition, are based on wave velocity and the information about the frequency content is not utilized. However, wave velocity techniques fail when the goal is to detect damage in the early stages. To overcome this issue, new techniques based on phase velocity and material damping [1,2] were developed. These techniques need proper identification of a frequency content transferred to a tested material. In practical/field applications, access to a structure is often limited to one side only (i.e. concrete slabs, vacuum building walls). Thus, surface wave analysis is a natural solution.

So far, the surface wave-based methods have been successfully applied for the characterization of the surface crack depth and quality of repair [3, 4]. Krstulovic-Opara et al. [5] showed that based on the surface wave dispersion, it is possible to determine stiffness profiles within structural elements and monitor the curing of concrete with respect to depth.

* Corresponding author: pwiciak@uwaterloo.ca

The change in signal amplitude of more than 95% was reported by Aggelis et al. [6] when cracked specimens were compared with sound ones. Chi-Won et al. [7] used surface waves (the responses were measured with ultrasonic transducers and microphones) for the characterization in asphaltic concrete. Finally, non-contact sensing techniques were applied for the reception of surface waves. Ham et al. [8] used a silicon-based miniature MEMS acoustic array located at a few millimetres from concrete cover.

However, the detailed frequency content that is transferred to the tested medium has been disregarded. Additionally, responses are usually measured with ultrasonic transducers, which do not have a flat frequency response.

This research is focused on identifying the frequency content of ultrasonic transducers, measured in absolute units. Based on this information, responses measured with the flat response state-of-the-art Doppler laser vibrometer are analyzed. The most sensitive vibration mode is extracted from the recorded signal with the wavelet synchro-squeezed transform (WSST). The methodology includes the characterization of the ultrasonic transducer performed with the laser Doppler vibrometer. The responses are measured along the transducer's diameter, and the resonant frequencies are defined from amplitude spectra. Void presence detection is performed based on the amplitude approach. Effectiveness of the methodology is verified based on the relative attenuation index calculated for three cases: full spectral range, spectral ranges centred at the resonant frequencies, and of signals obtained from the WSST techniques.

3 Methodology and laboratory setup

The methodology presented in this study consist of three steps. Firstly, the wear surface of the 54-kHz P-wave ultrasonic transducer, which is used in the transmission mode during the experiment, is scanned with the Doppler laser vibrometer. Based on the performed characterization, it is possible to select frequency ranges that will be studied in detail. In the next phase, two series of measurements are taken on the cemented sand specimen. The first line of measurements goes through the sound section of the specimen, while the other one goes on top of the subsurface void. In the third step, the signal processing of the recorded data is performed. Two groups of analysis are considered. Firstly, original time signals are analyzed, and damage index based on spectral areas is proposed. Next, the WSST technique is used to extract the most sensitive vibration modes, which are further analyzed in the same way as the original time signals. Finally, both approaches are compared, and conclusions are given.

3.1 Transducer characterization

The 54-kHz P-wave ultrasonic transducer used in this study in the transmission mode is firstly scanned with the laser vibrometer. In the characterization setup (Figure 1-a), a function generator (HP33120A) is used to provide an input signal (5V, 54 kHz square pulse). The response is read with a laser sensor head (LSH, Polytec OFV-534), which is connected to the vibration controller (OFV-2570). For the 54-kHz transducer (50 mm diameter), responses are measured at 45 positions distributed evenly (with a 1mm spacing) along its diameter.

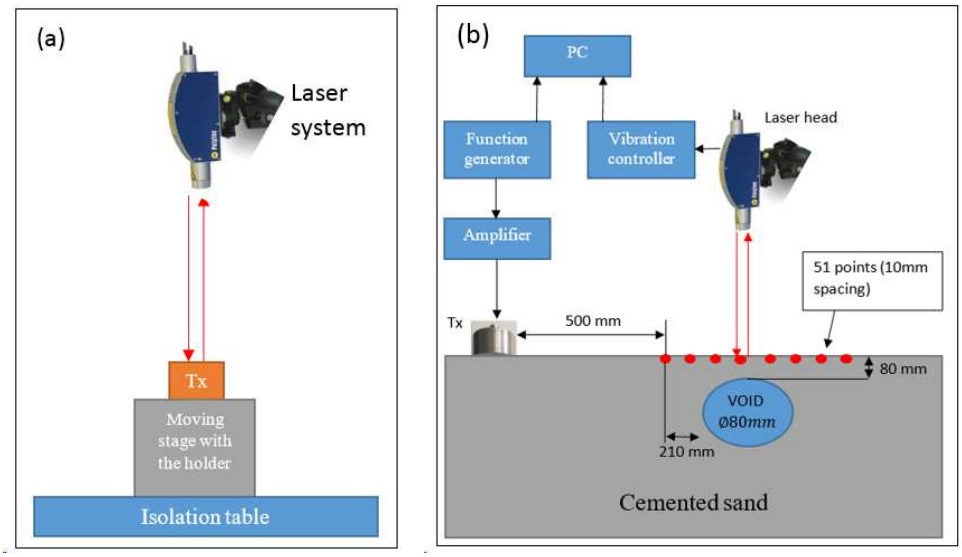

Fig. 1. Laboratory setups used in this study: (a) Transducer characterization setup and (b) cemented sand data collection setup.

3.2 Specimen preparation and data registration

The proposed methodology is developed and tested on a cemented sand medium (made of silica sand [Barco #71] mixed with about 10% by weight gypsum cement. The particle size distribution of the sand is given as D_{10} = 0.12 mm, D_{50} =0.18 mm, C_u = 1.8, and C_c = 1.04. The details of the properties can be found in Khan et al. [9]. The cemented sand has a depth of 300 mm and lateral dimensions of 1060x870 mm. The cemented sand lies on top of dry sand (450 mm thick) and is bounded by the chipboard box (with 60 mm-thick styrofoam inner-isolation). Considering the nominal frequency used in the test (54 kHz) and observed wave velocity (1183 m/s), the medium is considered as homogeneous. During the preparation of the specimen, a void was embedded at the central section of the box (a balloon with a diameter of 80mm was placed, thus the distance from the top surface to the top of the balloon is 80mm). The ultrasonic transmitter (54-kHz P-wave transducer made by Proceq) is placed on the surface of the cemented sand 50 mm away from the edge (along the mid-section, Figure 1-b). The function generator (HP33120A) provides an input signal (5V, 54 kHz square pulse), which is amplified to the amplitude ±125V. The responses are read with a laser sensor head (LSH, Polytec OFV-534), which is connected to the vibration controller (OFV-2570), similarly to the characterization setup. Two measurement lines are used. The intact line goes 80 mm to the side of the void edge, and the void line goes directly through the void. The response is measured at 51 locations (with 10 mm spacing) for both lines, and the first response is measured 500 mm away from the transmitter. Therefore, the void is located 210 mm away from the first reception position.

3.3 Signal processing techniques

In this study, the measured responses are analyzed in time and frequency domains separately. Additionally, the wavelet synchrosqueezed transform (WSST) is used, which transforms a time signal *x(t)* into the time-frequency domain and enables the decomposition of complex signals into the individual frequency component $x_i(t)$. First, similarly to continuous wavelet transform, wavelet coefficients are calculated $W_x(a,b)$, where a is the scale, and b is the time offset. For each point (a,b) an instantaneous frequency $\omega_x(a,b)$ is computed by

$$\omega_x(a,b) = -i\big(W_x(a,b)\big)^{-1}\frac{\partial}{\partial b}W_x(a,b). \quad (1)$$

Then, the time-scale plane is mapped $[(b,a)\rightarrow(b,\omega_x(a,b))]$ to the time-frequency with an operation called synchrosqueezing. The synchrosqueezing transform $T_x(\omega_{l,b})$ is given by

$$T_x(\omega_l,b) = (\Delta\omega)^{-1}\sum_{a_k:|\omega(a_k,b)-\omega_l|\leq\Delta\omega/2} W_x(a_k,b)\,{a_k}^{-3/2}(\Delta a)_k \quad (2)$$

where a_k are discrete values of the scale, $(\Delta a)_k=a_k-a_{(k-1)}$, frequencies ω_l are centres of the bins $[\omega_l-1/2\ \Delta\omega,\omega_l+1/2\ \Delta\omega]$ and $\Delta\omega=\omega_l-\omega_{(l-1)}$. If the individual components are well-separated [10], they can be estimated by inverting the synchrosqueezing transform

$$x_i(t) = \Re e\big(C_\psi^{-1}\textstyle\sum_l T_x(\omega_l,b)\big) \quad (3)$$

where $Re(.)$ defines the real part of the function, and the C_ψ is the normalization constant. In this study, the WSST methodology implemented in the synchrosqueezing toolbox in Matlab is used (with Morlet wavelet). More explanation of the WSST technique can be found in Daubechies et al. and Thakur et al. [10, 11].

To give the quantitative parameter, enabling separation between intact and damaged conditions, the relative attenuation term is introduced. It measures the percentage difference of energies measured for two different material conditions with respect to the intact condition. The relative attenuation is calculated as

$$Att = 100 * {(E_{INT} - E_{DAM})}/{E_{INT}} \quad (4)$$

where E_{INT} and E_{DAM} are signal energies computed for the initial and damaged (or changed over time) conditions.

4 Results and data analysis

In the next sections, results of transducer characterization and analysis of measured signals based on the original time signals and modes extracted with the WSST technique will be discussed.

4.1 Ultrasonic transmitter characterization

The knowledge of the transmitted signal is critical in the analysis of ultrasonic data. Not only it helps to understand the frequency content of the signals, but it can help to identify the wavelength of waves penetrating the tested material. Firstly, a wear surface of the 54-kHz transmitter is scanned with the laser vibrometer. Figure 2-a presents typical displacements (the amplitudes are normalized with respect to the maximum amplitude observed along the diameter) measured along the transducer diameter. Most of the energy (i.e. the largest displacement) is observed in the central section of the diameter. Therefore, a midpoint is selected to represent the transmitted frequency content.

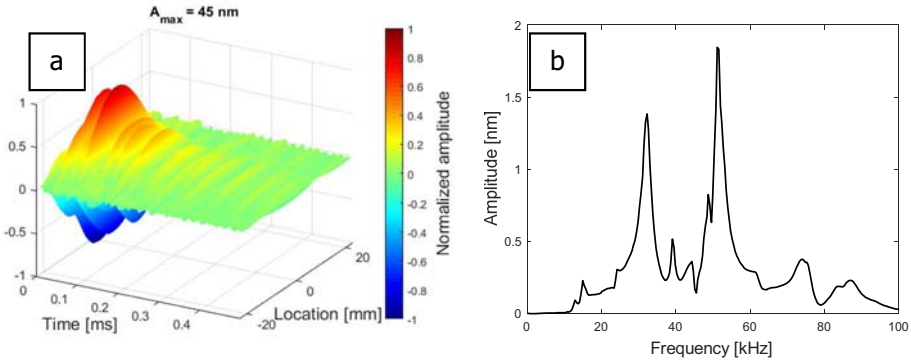

Fig. 2. Typical results obtained during characterization: (a) Time signals recorded along the diameter of the 54-kHz transmitter. The responses are normalized globally, and (b) the spectra of the signal recorded at the centre.

The analysis of the spectra presented in Figure 2-b reveals that in addition to the nominal resonant frequency, there are other frequencies present in the signal. The second significant peak is present at 32 kHz. Less prominent peaks can also be distinguished (16 and 39 kHz). These frequencies would normally be disregarded. Based on this information, the 32-kHz mode (which will be called 30-kHz mode for simplicity) will be extracted from the received signals using the WSST technique in the next chapters.

4.2 Analysis of original time signals

The group of analysis is performed on the original time signals. Figure 3-a presents time signals for the reference line (intact condition), while Figure 3-b shows time signals for the line placed on top of the void. Blue marks show the window that is applied before the fast Fourier transform is calculated. The amplitude spectra of the windowed signals are presented in Figure 3-c (intact) and Figure 3-d (damaged). The traditional wave velocity-based approach is not sensitive for the localized damage detection, as no significant change is observed for the inclination of the first arrival line. However, a sharp drop of signal amplitude is observed when the measuring point lies on top of the void (locations 20-30 in Figure 3-b). A similar effect is observed in the frequency domain. Although the two lines have different frequency content (due to the boundary effects, present even in the windowed signals), a distinct drop in spectral amplitude is observed in the void-line case. Moreover, the intact line

keeps the frequency character constant over the measurement array, while for the void line, the frequency content is modified when the measuring point passes the void.

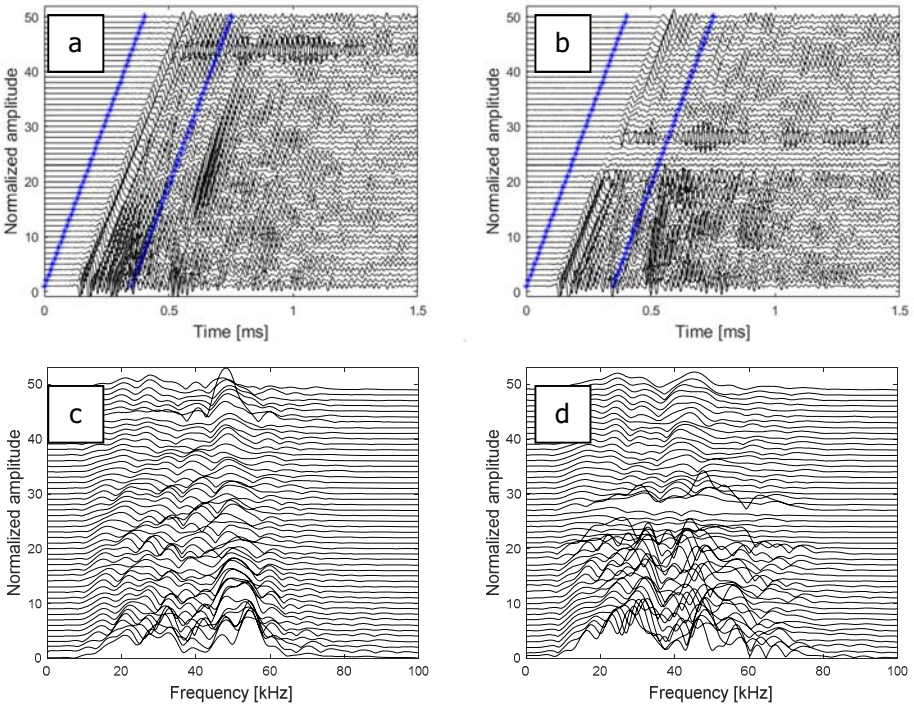

Fig. 3. Original time signals and frequency spectra (windowed signals) measured respectively (a and c) intact line and (b and d) void-line.

The visual analysis identifies the presence of the void. However, a quantitative parameter is needed. Therefore, the attenuation factor (defined in equation 4) is used. For each location, the relative energy difference based on spectral energy is calculated and presented in Figure 4. The energy is calculated based on the whole spectral range (blue colour in Figure 4), the frequency range of 30±10kHz, and the range 50±10kHz (the ranges are centred around the significant resonances presented in Figure 2). Three significant levels can be distinguished, and the 30-kHz frequency bin shows the least variability (the 30-kHz mode penetrates deeper into the material), and the comments will be presented based on this vibration mode. Before the void (locations 0-20), the relative attenuation fluctuates around zero, which means that the amplitudes for both lines are similar. When the wave reaches the void (locations 20-30) the amplitude in the void line is distinctly lower and the attenuation factor reaches the mean value of 78%. Finally, after the void, the amplitude is less affected (43%); however, it does not retrieve the values seen in the intact line.

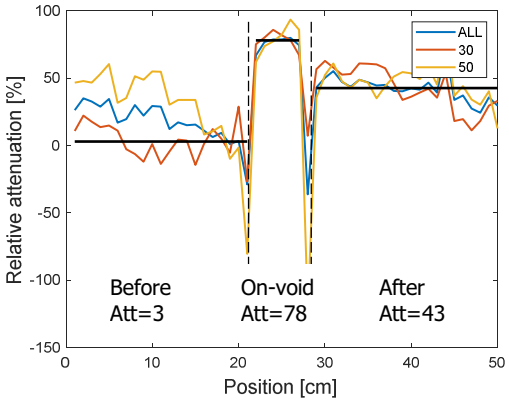

Fig. 4. Relative attenuation between two conditions calculated for different spectral cases. Blueline (full spectral range), red line (30 kHz), and yellow line (50 kHz). The mean relative attenuation values for the 30 kHz range are given for three sections: before the void (before), on top of the void (on-void), and after the void (after).

4.3 Analysis of 30-kHz mode extracted with WSST

In the next phase, signals shown in Figure 3 are subjected to the wavelet synchro-squeezing transform. A typical instantaneous frequency plot is shown in Figure 5. The amplitude is oversaturated purposely, highlighting the spectral position of the ridges (solid red lines) that are used for the extraction of modes. Only mode 30 is analyzed in the section.

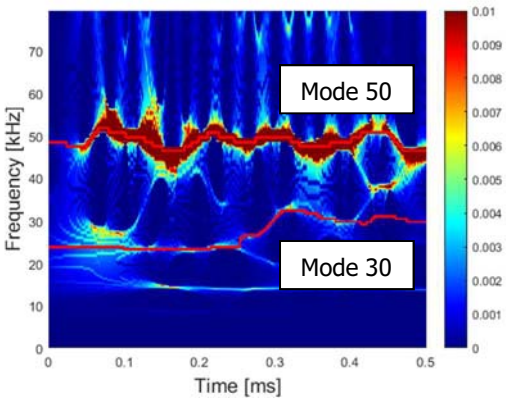

Fig. 5. Typical instantaneous frequencies estimated with the WSST technique. Red solid lines represent the ridges that are used in the reconstruction of mode signals .

Figure 6 presents a similar set of data, as shown in Figure 3; however, it is obtained for mode 30. It can be seen that the displacement is strongly associated with the arrival of the wave, and the reflections do not play as significant role as before. The same attenuation in amplitudes is observed. Another benefit of using the mode is that the frequency is narrowed and it is simpler to keep track of the changes that happen after the wave leaves the void.

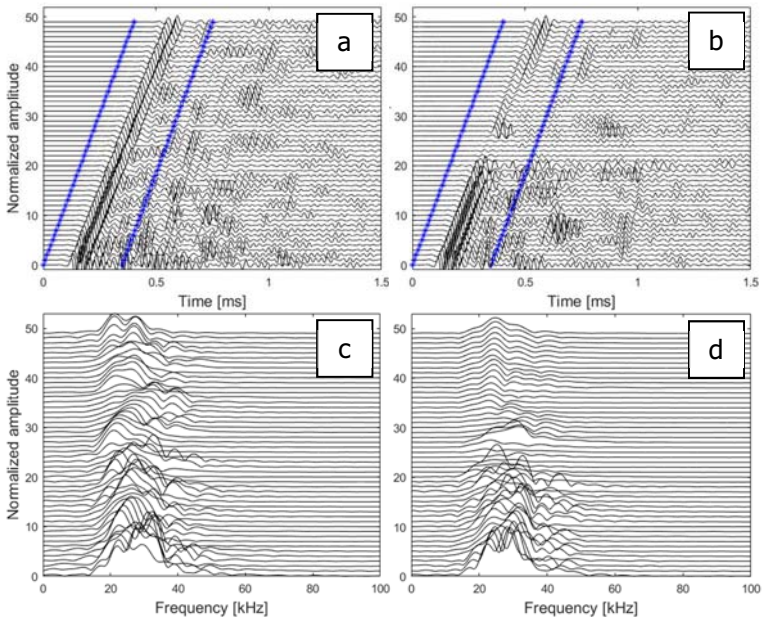

Fig. 6. Mode-30 time signals and frequency spectra (windowed signals) measured for (a and c) the intact line and (b and d) void-line.

The relative attenuation plot is repeated for the mode 30 signals and is presented in Figure 7. The negative values observed before the void (relative attenuation of -9%) mean that the amplitude in the void-line is higher (the differences come from the different boundary effects for both lines). A sharp drop (up to 70 %) is seen for location 20-30, and finally, after the void, the relative attenuation is lower (with the mean value of 39%). The frequency band gives very similar values as the energy calculated for the whole spectral range, which means that the mode extraction acts as a band-pass filter.

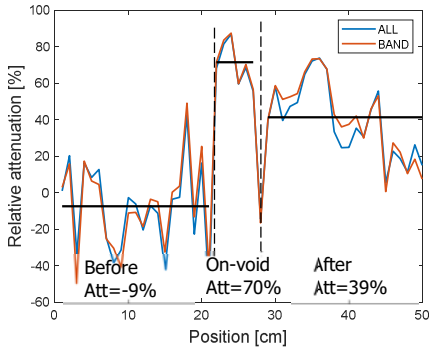

Fig. 7. Relative attenuation between two conditions calculated for mode 30 signals. Blueline (full spectral range), red line (30 kHz).

4.5 Summary of results

Finally, the results of both methods are compared. For each method, differences between mean relative attenuation values on-void and before-void, on-void and after-void, and after-before-void are calculated and presented in Table 1. The difference between relative attenuation after and before the void measures the permanent loss of energy, even when the measuring point is to the side of the void. The approach based on the original time signals and whole spectral range is considered as a reference point for the modified method based on the WSST technique.

Table 1. Relative attenuation differences for different positions with respect to the void location.

		Relative attenuation difference [% points]		
Method	Frequency range	On - before	On - after	After - before
Original signals	Whole range	58	33	25
	30±10kHz	75	35	40
	50±10kHz	50	33	17
Mode 30	Whole range	79	31	48
	30±10kHz	79	30	49

It can be concluded that the separation between the before and on top of the void conditions, obtained based on the full spectral range is not sufficient (58% points). The results can be improved by narrowing the analyzed range of frequencies. However, one has to perform that carefully. Only mode 30 provides the improvement (75% points) in the proper condition characterization (mode 50 is less sensitive and is responsible for low separation value).

Further improvements can be obtained with the help of the WSST technique. The extraction of the pure 30-kHz mode increases the separation between two conditions to 79% points. For all methods, when the measuring point is located after the void, the amplitude is slightly restored (by approximately 30 percentage points) than when directly on top of the void. Additionally, for both methods analyzing 30 kHz mode, it can be seen that the loss of energy is permanent, and even when the measuring point passes the void, the amplitude is 40-50 percentage points lower than for the reference (intact) line.

5 Conclusions

In this study, the authors start the condition assessment procedure for cementitious materials by the characterization of the ultrasonic transducer used in the tests. The wear surface is scanned with the state-of-the-art Doppler laser vibrometer. Based on the spectral analysis, two vibration modes are considered. The evaluation procedure is done in two steps. First, the original time signals are analyzed (both in time and frequency domains), and the relative attenuation factor is proposed and used based on spectral energies. In the second step, the WSST technique is used to extract the 30-kHz vibration mode (which penetrates deeper into the specimen). The same time and frequency analyses are repeated for the mode-signals. Finally, both approaches are compared. It has been shown that the proposed methodology can successfully be used for the condition assessment for specimens with localized damage, and the following conclusions can be given.

1. The scans of response along the transmitter diameter and globally-normalized signals revealed that the majority of energy is sent at the centre of the wear surface. The analysis of the vibration at the centre showed an additional frequency component other than the nominal resonant frequency. Therefore, detailed information about the frequency content transferred to the tested medium was obtained. The possible application of the characterization procedure includes improved FEA modelling (with detailed and more accurate excitation information).
2. Analysis of the original time signals showed no significant wave velocity change with the presence of the void in one of the measuring lines. However, distinct amplitude changes were observed when the measuring point was located on top of the void. The relative attenuation factor was calculated based on spectral energy. Additionally to the full spectral range, based on the transducer characterization, two frequency ranges centred at the resonant frequencies were proposed. It has been shown that the 30-kHz range is more sensitive to damage detection.
3. Using vibration mode extraction techniques (e.g. the WSST), it is possible to analyze only the precisely filtered signals. The WSST was applied to the measured signals, and the 30-kHz mode was extracted. The procedure was repeated as for the group of original time signals. The same amplitude character of void presence was observed. However, due to the filtered nature of signals, it is easier to analyze the changes in the frequency content of the signals due to the void presence.
4. Finally, two approaches were compared. The basic calculation of the relative attenuation index can be improved by analyzing only the sensitive part of spectra (the assessment can be improved by 17 percentage points with respect to the basic calculation). Further improvement was obtained applying the WSST technique, and the WSST-based assessment was improved by 21 percentage points when compared to the basic evaluation.

Acknowledgment

The authors would like to acknowledge the financial support from the Natural Sciences and Engineering Council of Canada (NSERC) and OPG/UNENE through the NSERC-CRD program.

References

1. Y. Yang, G. Cascante, M. A. Polak, NDT&E Int. **42**, 501-512 (2009).
2. A. Kirlangic, G. Cascante, M. A. Polak, ACI Mat. J. **113**, 73-82 (2016).
3. D. G. Aggelis, T. Shiotani, Cem. & Con. Comp. **29**, 700-711 (2007).
4. D. G. Aggelis, T. Shiotani, D. Polyzos, Cem. & Con. Comp. **31**, 77-83 (2009).
5. N. Krstulovic-Opara, R. D. Woods, N. Al-Shayea, ACI Mat. J. **93**, 75-86 (1996).
6. D.G. Aggelis, E.Z. Kordatos, M. Strantza, D.V. Soulioti, T.E. Matikas, Con. And Build. Mat. **25**, 3089-3097 (2011).
7. C.-W. In, J.-Y. Kim, K. E. Kurtis, L. J. Jacobs, NDT&E Int. **42**, 610-617 (2009).
8. S. Ham, H. Song, M. L. Oelze, J. S. Popovics, Ultrasonics **75**, 46-57 (2017).
9. Z. Khan, A. Majid, G. Cascante, D. J. Hutchinson, P. Pezeshkpour, Can. Geotech. J. **43,** 294–309 (2006).
10. I. Daubechies, J. Lu, H.-T. Wu, Appl. Comput. Harmon. Anal. **30**, 243-261 (2011).
11. G. Thakur, E. Brevdo, N. S. Fuckar, H.-T. Wu, Signal Processing **93,** 1079–1094 (2013).